Available online at www.sciencedirect.com
SCIENCE DIRECT®
Journal of Sound and Vibration 287 (2005) 315–328
JOURNAL OF SOUND AND VIBRATION
www.elsevier.com/locate/jsvi

A spectral super element for modelling of plate vibration. Part 2: turbulence excitation

F. Birgersson, S. Finnveden*

MWL, Aeronautical and Vehicle Engineering, KTH, SE-100 44 Stockholm, Sweden

Received 2 February 2004; received in revised form 1 June 2004; accepted 4 November 2004
Available online 18 January 2005

Abstract

In the accompanying paper, the suitability of a spectral super element to predict the response to point force excitation, was demonstrated. This paper expands the element formulation to also include distributed forces, which is useful when studying distributed excitation. First the sensitivity function, i.e. the structural response to a travelling pressure wave, is found. This sensitivity function and a wavenumber frequency description of the wall pressure are then used to predict the response of a turbulence excited panel in a numerically efficient way. The predictions were validated by a conventional finite element method and also compared to measurements.

1. Introduction

The noise generated by turbulent boundary layer (TBL) flow over the surface of fast moving vehicles such as aircraft, trains and ships, remains a source of annoyance. These vehicles are often very large, whereas the length and time scales of the excitation may be comparatively small, which often implies impossibly large computer models for the prediction of noise and vibration.

One advantage, when modelling these vehicles, is that they are often built up of simpler structures, such as curved plates. The spectral super element method (SSEM) in the accompanying paper [1] was developed to handle exactly this type of structures and to predict the structural

*Corresponding author.
E-mail addresses: svantef@kth.se (F. Birgersson), svantef@kth.se (S. Finnveden).

0022-460X/$ - see front matter © 2004 Elsevier Ltd. All rights reserved.
doi:10.1016/j.jsv.2004.11.011

vibration with a high computational efficacy. The spectral super elements can also be put into an assembly with conventional finite elements, which is convenient whenever small and more complicated parts, e.g. stringers and frames, are modelled with such elements instead.

With the finite element method, a distributed force is sometimes a bit carelessly considered as a set of point forces acting on the structure. This approximation will usually not cause much error as long as the force is a slowly varying function over each finite element. With the SSEM, however, this is not a possible approach as the force will normally vary to a great extent over the surface of these relatively large elements. In this paper, the theory of Part 1 is extended to handle distributed forces, which is advantageous as it increases the applicability of the method greatly.

More specifically, the structural response to a travelling pressure wave derived here is also referred to as the sensitivity function of the structure by Newland [2] and Lin [3]. Once found, it can be used to efficiently predict the structural response to homogeneous, stationary, random excitation, namely as an integral of the cross-spectral density of the excitation and the sensitivity function in the wavenumber domain. This fact has been used successfully before in for example Refs. [4–6] to predict turbulence-induced vibration and will be explored here in conjunction with the developed spectral super element.

Two models will be used to describe the wall pressure excitation of a turbulent boundary layer flow in this paper, a Chase [7] and a Corcos model [8], both modified as presented in Ref. [9]. These two models differ mainly in the way they describe the low wavenumber domain of the TBL, which in turn implies differences in predicted structural response above a certain frequency. This difference is discussed in more detail in Ref. [9] and will only be mentioned briefly here.

The paper starts with an element formulation for a distributed force and then derives the sensitivity function. This sensitivity function is validated against an exact spectral finite element method (SFEM) and then used to predict the response to turbulence excitation. Finally, these results are validated against predictions using a detailed finite element method and also against measurements in a wind tunnel.

2. Element formulation for a distributed force

In this section the sensitivity function is derived. It is the structural response of the structure to a travelling pressure wave.

2.1. Displacement functions

Consider a plate of length L_x and width L_y that is located in the xy plane. It is excited by a distributed force of the form of a travelling pressure wave

$$p(x,y,t) = p_0\, \mathrm{e}^{-\mathrm{i}\alpha_x x}\mathrm{e}^{-\mathrm{i}\alpha_y y}\mathrm{e}^{\mathrm{i}\omega t}, \tag{1}$$

where $\alpha_{x,y}$ are wavenumbers, ω is angular frequency and p_0 is pressure amplitude. The structural response to this pressure is given by a homogeneous solution and a particular solution. The homogeneous solution is detailed in Ref. [1, Eq. (23)] and the particular solution is derived in what follows. To that end, the virtual work of a distributed force is included in the Lagrangian

[1, Eqs. (16) and (33)]

$$\begin{aligned} L &= \int\int \boldsymbol{\varepsilon}^{a\mathrm{T}}\mathbf{C}\,\boldsymbol{\varepsilon} - \omega^2\rho h\,\mathbf{u}^{a\mathrm{T}}\mathbf{u} - p^*w - pw^a\,\mathrm{d}y\,\mathrm{d}x \\ &= \int \sum_{m=0}^{2}\sum_{n=0}^{2} \frac{\partial^m \mathbf{V}^{a\mathrm{T}}}{\partial x^m}\boldsymbol{\varepsilon}_{mn}\frac{\partial^n \mathbf{V}}{\partial x^n} - \omega^2\mathbf{V}^{a\mathrm{T}}\mathbf{m}_{00}\mathbf{V}\,\mathrm{d}x \\ &\quad + \int\int -p^*w - pw^a\,\mathrm{d}y\,\mathrm{d}x, \end{aligned} \tag{2}$$

where ρ and h are density and thickness of the plate, respectively. $\mathbf{C}$ is the rigidity matrix and vector $\boldsymbol{\varepsilon}$ contains the components of strain, which are linear functionals of the displacement $\mathbf{u}$ and its spatial derivatives. $\boldsymbol{\varepsilon}_{mn}$ and $\mathbf{m}_{00}$ are assembled matrices from Ref. [1, Eq. (15)]. The components of $\mathbf{V}$ are the nodal dof at the element ends. Similar to Part 1, the plate is subdivided into a number of plate strips. In each strip element j, the dependence of the displacement in the z-direction is described by a vector of polynomials $\mathbf{f}$ and is a linear function of the nodal dof $\mathbf{V}_j(x)$ [1, Eq. (8)]

$$w_j(x,y) = \mathbf{f}\,\mathbf{C}_w\mathbf{V}_j(x), \tag{3}$$

where $\mathbf{f} = (1 \quad y/l_y \quad (y/l_y)^2 \quad (y/l_y)^3)$ and the projection matrix $\mathbf{C}_w$ is defined in Ref. [1, Eq. (11)]. Substituting Eqs. (3) and (1) into Eq. (2), it is possible to element wise evaluate the integral with respect to y as

$$\int\int -p^*w - pw^a\,\mathrm{d}y\,\mathrm{d}x = \int_{-l_x}^{l_x} (-\mathbf{P}^{*\mathrm{T}}(\alpha_y)\mathbf{V}(x) - \mathbf{V}^{a\mathrm{T}}(x)\mathbf{P}(\alpha_y))\mathrm{e}^{-\mathrm{i}\alpha_x x}\,\mathrm{d}x, \tag{4}$$

where $\mathbf{P}(\alpha_y)$ is found from assembling $\mathbf{P}_j(\alpha_y)$ below from each strip element

$$\mathbf{P}_j(\alpha_y) = \mathrm{e}^{-\mathrm{i}\alpha_y y_j}\mathbf{C}_w^{\mathrm{T}}\int_{-l_y}^{l_y} \mathbf{f}^{\mathrm{T}}\mathrm{e}^{-\mathrm{i}\alpha_y y}\,\mathrm{d}y. \tag{5}$$

y_j is the location of the elements local coordinate system with respect to the global. If the local coordinate system is shifted also in the x-direction, this has to be accounted for in Eq. (4). The integral Eq. (5) is evaluated exactly without any need for numerical quadrature.

If the displacement of the adjoint system $\mathbf{V}^{a\mathrm{T}}$ is varied in the Lagrangian (2), the following equation of motion is found

$$\left(\mathbf{A}_4\frac{\partial^4}{\partial x^4} + \mathbf{A}_2\frac{\partial^2}{\partial x^2} + \mathbf{A}_1\frac{\partial}{\partial x} + \mathbf{A}_0 - \omega^2\mathbf{M}\right)\mathbf{V}(x) = \mathbf{P}(\alpha_y)\mathrm{e}^{-\mathrm{i}\alpha_x x}, \tag{6}$$

where $\mathbf{A}_i$ are given by [1, Eq. (18)]

$$\mathbf{A}_4 = \boldsymbol{\varepsilon}_{22},\ \mathbf{A}_2 = \boldsymbol{\varepsilon}_{02} - \boldsymbol{\varepsilon}_{11} + \boldsymbol{\varepsilon}_{20},\ \mathbf{A}_1 = \boldsymbol{\varepsilon}_{01} - \boldsymbol{\varepsilon}_{10},\ \mathbf{A}_0 = \boldsymbol{\varepsilon}_{00},\ \mathbf{M} = \mathbf{m}_{00}.$$

It follows that the particular solution is given by

$$\mathbf{V}_p(x,\alpha_x,\alpha_y) = \boldsymbol{\Gamma}(\alpha_x,\alpha_y)\mathrm{e}^{-\mathrm{i}\alpha_x x}, \tag{7}$$

where

$$\boldsymbol{\Gamma} = (\mathbf{A}_4(-\mathrm{i}\alpha_x)^4 + \mathbf{A}_2(-\mathrm{i}\alpha_x)^2 + \mathbf{A}_1(-\mathrm{i}\alpha_x) + \mathbf{A}_0 - \omega^2\mathbf{M})^{-1}\mathbf{P}(\alpha_y). \tag{8}$$

Adding the homogeneous solution, derived in Part 1, and the particular solution, the displacement in the waveguide can be expressed as a function of the nodal displacement $\mathbf{W}$ in a similar fashion as described in Ref. [1, Section 3.1],

$$\mathbf{V}(x) = \mathbf{\Phi}\mathbf{E}(x)\mathbf{A}(\mathbf{W} - \mathbf{W}_p) + \mathbf{V}_p(x), \tag{9}$$

where the components of $\mathbf{W}_p$ are the values of the particular solution and its derivative at the nodes of the element, given by

$$\mathbf{W}_p = \begin{pmatrix} \mathbf{B}_1\mathbf{V}_p(-l_x) \\ \mathbf{B}_2(-\mathrm{i}\alpha_x)\mathbf{V}_p(-l_x) \\ \mathbf{B}_3\mathbf{V}_p(+l_x) \\ \mathbf{B}_4(-\mathrm{i}\alpha_x)\mathbf{V}_p(+l_x) \end{pmatrix}. \tag{10}$$

$\mathbf{B}_i$, $\mathbf{\Phi}$ and $\mathbf{A}$ are detailed in the companion paper [1]. The entries of the diagonal matrix $\mathbf{E}$ are given by

$$(\mathbf{E})_{ii} = \mathrm{e}^{\kappa_{ii}x - (\kappa_p)_{ii}l_x}, \tag{11}$$

where κ is a diagonal matrix of eigenvalues and κ_p is a scaling matrix, see Ref. [1, Eq. (21)].

2.2. Sensitivity function

The displacement functions are expressed by Eq. (9). Similarly, the complex conjugate of the displacement functions for the adjoint system are by symmetry given as

$$\mathbf{V}^a(x) = \mathbf{\Phi}\mathbf{E}(x)\mathbf{A}(\mathbf{W}^a - \mathbf{W}^a_p) + \mathbf{V}^a_p(x), \tag{12}$$

where $\mathbf{W}^a_p$ and $\mathbf{V}^a_p$ are found in the same way in the previous section. The Lagrangian (2) is evaluated by substituting the components of $\mathbf{V}$ and $\mathbf{V}^a$ into it.

$$\begin{aligned} L = \int_{-l_x}^{l_x} \sum_{m=0}^{2}\sum_{n=0}^{2} & \mathbf{W}^{a\mathrm{T}}\mathbf{A}^{\mathrm{T}}\frac{\partial^m \mathbf{E}(x)}{\partial x^m}\mathbf{\Phi}^{\mathrm{T}}\boldsymbol{\varepsilon}_{mn}\frac{\partial^n}{\partial x^n}(\mathbf{\Phi}\mathbf{E}(x)\mathbf{A}(\mathbf{W} - \mathbf{W}_p) + \mathbf{\Gamma}\mathrm{e}^{-\mathrm{i}\alpha_x x}) \\ & - \omega^2\mathbf{W}^{a\mathrm{T}}\mathbf{A}^{\mathrm{T}}\mathbf{E}(x)\mathbf{\Phi}^{\mathrm{T}}\mathbf{m}_{00}(\mathbf{\Phi}\mathbf{E}(x)\mathbf{A}(\mathbf{W} - \mathbf{W}_p) + \mathbf{\Gamma}\mathrm{e}^{-\mathrm{i}\alpha_x x}) \\ & - \mathbf{W}^{a\mathrm{T}}\mathbf{A}^{\mathrm{T}}\mathbf{E}(x)\mathbf{\Phi}^{\mathrm{T}}\mathbf{P}(\alpha_y)\mathrm{e}^{-\mathrm{i}\alpha_x x}\,\mathrm{d}x + R \\ = \mathbf{W}^{a\mathrm{T}}\mathbb{D}\mathbf{W} & - \mathbf{W}^{a\mathrm{T}}\mathbf{F}_1 - \mathbf{W}^{a\mathrm{T}}\mathbf{F}_2 - \mathbf{W}^{a\mathrm{T}}\mathbf{F}_3 + R, \end{aligned} \tag{13}$$

where R contains terms that do not depend on the variational parameter $\mathbf{W}^a$ and are of no interest here. Furthermore,

$$\mathbf{F}_1 = \mathbb{D}\mathbf{W}_p, \tag{14}$$

$$\mathbf{F}_2 = -\mathbf{A}^{\mathrm{T}}(\mathbf{\Theta}_{\alpha_x} .* \mathbf{E}_{\mathbf{I}\alpha_x}), \tag{15}$$

$$\mathbf{F}_3 = \mathbf{A}^{\mathrm{T}}(\mathbf{\Phi}^{\mathrm{T}}\mathbf{P}(\alpha_y) .* \mathbf{E}_{\mathbf{I}\alpha_x}), \tag{16}$$

$$\mathbf{\Theta}_{\alpha_x} = \left(\sum_{m=0}^{2} \sum_{n=0}^{2} (\kappa^m (\mathbf{\Phi}^{\mathrm{T}} \boldsymbol{\varepsilon}_{mn} \mathbf{\Gamma})(-\mathrm{i}\alpha_x)^n) - \omega^2 (\mathbf{\Phi}^{\mathrm{T}} \mathbf{m}_{00} \mathbf{\Gamma}) \right), \tag{17}$$

$$\mathbf{E}_{\mathbf{I}\alpha_x} = \int_{-l_x}^{l_x} (\operatorname{diag} \mathbf{E}(x)) \mathrm{e}^{-\mathrm{i}\alpha_x x} \, \mathrm{d}x. \tag{18}$$

The dynamic stiffness matrix $\mathbb{D}$ is given by Ref. [1, Eq. (29)]. The operator diag produces a column vector from its arguments main diagonal and .* denotes element wise multiplication. The integral in Eq. (18) is evaluated analytically as in Ref. [4, Eq. (A7)]. By requiring that the first variation of this Lagrangian with respect to the variational parameter is zero, a system of equations for the nodal displacement $\mathbf{W}$ is found,

$$\mathbb{D}\mathbf{W} = \mathbf{F}, \tag{19}$$

where the nodal force vector $\mathbf{F}$ is given by

$$\mathbf{F} = \mathbf{F}_1 + \mathbf{F}_2 + \mathbf{F}_3. \tag{20}$$

The dynamic stiffness matrix $\mathbb{D}$ does not depend on the excitation and for a general source, described by a superposition of pressure wave excitations, it is therefore only the nodal force vector that needs to be recalculated.

Solving Eq. (19) gives the nodal displacements $\mathbf{W}$ of the structure, when excited by a pressure wave $p_0 \mathrm{e}^{-\mathrm{i}\alpha_x x} \mathrm{e}^{-\mathrm{i}\alpha_y y}$. The displacement within the element is then described by Eq. (9) and for future reference, the response to a pressure wave with $p_0 = 1\,\mathrm{N/m^2}$ will here be denoted by the sensitivity function G. This function may, similar to Newland [2, Chapter 16], also be expressed as an integral

$$G(\mathbf{r}, \alpha_x, \alpha_y, \omega) = \int_S H(\mathbf{r}, \mathbf{s}, \omega) \, \mathrm{e}^{-\mathrm{i}\alpha_x x_s} \mathrm{e}^{-\mathrm{i}\alpha_y y_s} \, \mathrm{d}\mathbf{s}, \tag{21}$$

where $\mathbf{r} = (x, y)$ and $\mathbf{s} = (x_s, y_s)$. S is the surface of the structure and $H(\mathbf{r}, \mathbf{s}, \omega)$ represents the response at location $\mathbf{r}$ to a harmonic point load of unit magnitude at location $\mathbf{s}$.

2.3. Validation of sensitivity function

In order to validate the previously derived element formulation (19), a comparison was made to the results from an exact spectral finite element [4]. The geometric and material properties of the investigated plate is described in Section 4.1. The damping was here described by a complex Young's modulus, $E(1 + \mathrm{i}\eta)$, with η equal to 0.02. The plate was chosen to be simply supported, since, similar to an exact dynamic stiffness method [10], the exact spectral finite element [4] requires at least two opposite edges to be simply supported.

Fig. 1 shows the velocity response of the plate at a point $(L_x/4, 3L_y/9)$, when excited by a travelling pressure wave (1) with $\alpha_x = 2.5\,\mathrm{m^{-1}}$ and $\alpha_y = 3\,\mathrm{m^{-1}}$. The results with the SSEM and SFEM agree very well, except above 900 Hz, where a small error is noticeable, which then grows above 1500 Hz. Around these two frequencies, the fifth- and sixth-order transverse modes cut on and with only nine assembled element strips used in the SSEM, these transverse modes could only be approximated. With more elements, on the other hand, the convergence of the results was

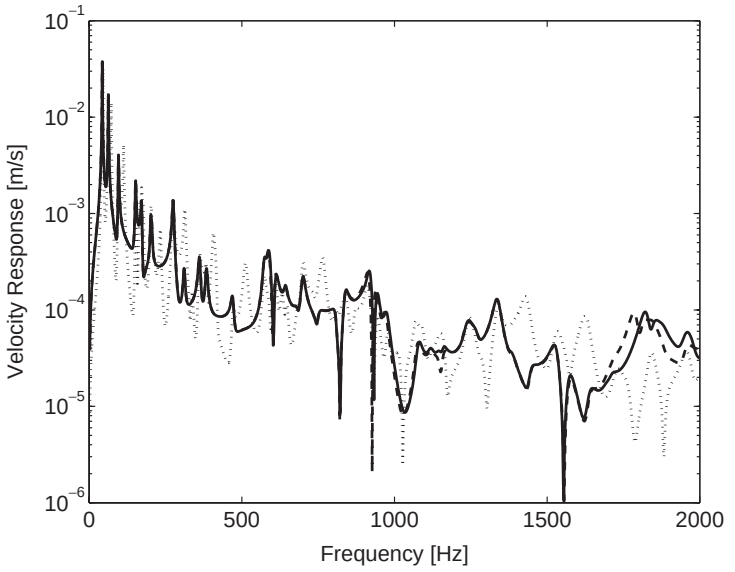

Fig. 1. Velocity response of simply supported plate excited by a travelling pressure wave with $\alpha_x = 2.5\,\mathrm{m}^{-1}$, $\alpha_y = 3\,\mathrm{m}^{-1}$. Solid, exact solution with an exact SFEM; dashed, SSEM; dotted, SSEM with only homogeneous solution.

verified. The figure also shows the result obtained if the particular solution is ignored in the element formulation. Ignoring this part of the solution simplifies the formulation greatly, e.g. $\mathbf{F}_1$ and $\mathbf{F}_2$ are then zero in Eq. (20). However, this approach can lead to significant errors especially within the element as shown in the figure and is not to be recommended.

3. Vibrational response to TBL excitation

3.1. Response to distributed random excitation

The response to distributed random excitation is given by Newland [2] as

$$S_{ww}(\mathbf{r}_1, \mathbf{r}_2) = \int_S \int_S H^*(\mathbf{r}_1, \mathbf{s}_1, \omega)\, H(\mathbf{r}_2, \mathbf{s}_2, \omega)\; S_{pp}(\mathbf{s}_1, \mathbf{s}_2, \omega)\, \mathrm{d}\mathbf{s}_1\, \mathrm{d}\mathbf{s}_2, \tag{22}$$

where the cross-spectral densities of the response and the pressure are defined by

$$\begin{aligned} S_{ww}(\mathbf{r}_1, \mathbf{r}_2, \omega) &= \langle w^*(\mathbf{r}_1, \omega), w(\mathbf{r}_2, \omega)\rangle, \\ S_{pp}(\mathbf{s}_1, \mathbf{s}_2, \omega) &= \langle p^*(\mathbf{s}_1, \omega),\; p(\mathbf{s}_2, \omega)\rangle. \end{aligned} \tag{23}$$

$\langle\ \rangle$ denotes statistical expectation. If the distributed excitation $p(\mathbf{s}, \omega)$ is assumed to be a sample function from a process, which is stationary and homogeneous in space, $S_{pp}(\mathbf{s}_1, \mathbf{s}_2, \omega)$ is a function of only the frequency and the spatial separations,

$$\xi_x = x_{s1} - x_{s2} \quad \text{and} \quad \xi_y = y_{s1} - y_{s2}. \tag{24}$$

3.2. Cross-spectral density of the pressure

Two different models will be used to describe the cross-spectral density of the pressure. They describe the wall pressure in a similar way around the convective peak, which is when the wavenumber in the streamwise direction equals the convective wavenumber. This convective wavenumber is defined by $k_c = \omega/U_c$, where U_c is the convection velocity. In the low wavenumber domain, however, the models differ significantly. As discussed in Ref. [9], this affects the structural response above the aerodynamic coincidence frequency. Hence, it is important to choose the model that not only describes the measured wall pressure field, but also enables accurate predictions of the structural response.

3.2.1. Modified Corcos' model

The pressure cross-spectrum is described by Corcos' model [8]

$$S_{pp}(\xi_x, \xi_y, \omega) = \Phi_{pp}(\omega)\, \mathrm{e}^{-c_x\, \omega\, |\xi_x|/U_c}\, \mathrm{e}^{-c_y \omega |\xi_y|/U_c}\, \mathrm{e}^{\mathrm{i}\, \omega \xi_x/U_c}, \tag{25}$$

where Φ_{pp} is the wall pressure power spectral density. c_x and c_y describe the spatial coherence of the wall pressure field in the longitudinal and transverse directions, respectively. In this work experimentally determined values as function of frequency were used for Φ_{pp}, c_x, c_y and U_c [9]. Thus, the model was made frequency and flow speed dependent in a similar way to Efimtsov's model [11]. The measured values for c_x and c_y were in fact described quite well by Efimtsov's model above 1000 Hz for the structure investigated here, see Ref. [9].

3.2.2. Modified Chase's model

Chase's model is believed to describe the low-wavenumber domain better than Corcos' model, which is important for the response prediction at higher frequencies. Chase's original model [7, Eqs. (72–74)] gave a reasonable description of the measured cross-correlation. However, as a slightly modified pressure cross-spectrum found in Ref. [9] provided a better agreement to the measurements, it will be used instead. For this modified model two more parameters, γ_M and γ_T, were introduced to better fit the transverse length scale to measurements. Furthermore, the relation between the term describing the self-noise and the one describing the shear noise was made frequency and flow speed dependent.

$$\begin{aligned} S_{pp}(\xi_x, \xi_y, \omega) = \Phi_{pp}(\omega)\{&\mathrm{A}_M(\omega, U_c)\mathrm{f}_M(\xi_x, \xi_y, \omega)\mathrm{e}^{-z_M}\mathrm{e}^{\mathrm{i}\, k_c\, \xi_x} \\ &+ \mathrm{A}_T(\omega, U_c)\mathrm{f}_T(\xi_x, \xi_y, \omega)\mathrm{e}^{-z_T}\mathrm{e}^{\mathrm{i}\, k_c\, \xi_x}\}, \end{aligned} \tag{26}$$

where

$$\mathrm{f}_M = 1 + z_M + \alpha_M^2 \mu_M^2 (1 - z_{M1}^2/z_M) + 2\mathrm{i}\alpha_M\, \mu_M\, z_{M1}, \tag{27}$$

$$\mathrm{f}_T = 1 + z_T + \alpha_T^2 \gamma_T^2 (1 - z_{T2}^2/z_T) + \alpha_T^2\, \mu_T^2 (1 - z_{T1}^2/z_T) + 2\mathrm{i}\alpha_T\, \mu_T\, z_{T1}. \tag{28}$$

$$z_{M1} = \mu_M \alpha_M k_c \xi_x, \quad z_{T1} = \mu_T \alpha_T k_c \xi_x, \tag{29}$$

$$z_{M2} = \gamma_M \alpha_M k_c \xi_y, \quad z_{T2} = \gamma_T \alpha_T k_c \xi_y, \tag{30}$$

$$\alpha_M = \sqrt{1 + (b_M k_c \delta)^{-2}}, \quad \alpha_T = \sqrt{1 + (b_T k_c \delta)^{-2}}, \tag{31}$$

$$z_M = \sqrt{z_{M1}^2 + z_{M2}^2}, \quad z_T = \sqrt{z_{T1}^2 + z_{T2}^2}. \tag{32}$$

The following model for the relative magnitudes $\mathrm{A}_{M,T}$ was postulated [9]

$$\begin{aligned} \mathrm{A}_M(\omega, U_c) &= (1 - r)/(1 + \alpha_M^2 \mu_M^2), \\ \mathrm{A}_T(\omega, U_c) &= r/(1 + \alpha_T^2 \gamma_T^2 + \alpha_T^2 \mu_T^2) \end{aligned} \tag{33}$$

with

$$r(\omega, U_c) = a(U_c) - b(U_c)\omega/\omega_0, \quad \omega_0 = 10^5 [\mathrm{rad/s}]. \tag{34}$$

r is restricted to take values between zero and one. The non-dimensional parameters μ_M, μ_T, γ_M, γ_T, b_T, b_M, a and b are determined as in Ref. [9] and are listed in Table 1 together with the boundary layer thickness δ. The values for b_T and b_M are similar to the default values given by Chase [7, Eq. (86)], whereas μ_M is almost twice as large and μ_T approximately three times smaller. This changes the length scales in the spanwise and streamwise directions, which is discussed further in Ref. [9]. It is noticeable that the parameters are all frequency independent and that only a, b and δ depend on the flow speed.

3.2.3. *Wavenumber description*

The cross-spectral density of the pressure can be expressed as an exponential Fourier series. The period of the exponential Fourier series has to be taken as at least twice the length and width of the plate, because integral (22) of x_{si} and y_{si} is over the length and width of the structure and thus ξ_x and ξ_y need to be evaluated in the interval $-L_x \ldots L_x$ and $-L_y \ldots L_y$, respectively. Outside this interval the cross-spectral density can be made periodic as any existing pressure outside the integration limits will not affect the result. Upon this basis the cross-spectral density is given by

$$S_{pp}(\mathbf{s}_1, \mathbf{s}_2, \omega) = \Phi_{pp}(\omega) \sum_{m=-\infty}^{\infty} \sum_{n=-\infty}^{\infty} \mathrm{S}_{PP}(\alpha_m, \alpha_n) \mathrm{e}^{\mathrm{i}\alpha_m \xi_x} \mathrm{e}^{\mathrm{i}\alpha_n \xi_y}, \tag{35}$$

where

$$\alpha_m = 2\pi m/2L_x, \quad \alpha_n = 2\pi n/2L_y. \tag{36}$$

The Fourier series coefficients $\mathrm{S}_{PP}(\alpha_m, \alpha_n)$ can be found analytically for Corcos' model, as in Ref. [4, Eqs. (39) and (40)]. It is however also possible to find these coefficients numerically with a 2D fast Fourier transform (FFT). This procedure is more general, as any type of description for the

Table 1
Parameters for modified Chase model

a[a]	b[a]	δ[a]	b_M	b_T	μ_M	μ_T	γ_M	γ_T
0.5928	0.1355	50 mm	0.5973	0.3158	0.2831	0.0614	1.2267	1.4186

[a] a, b and δ depend on flow speed; here values for 100 m/s are shown.

cross-spectral density of the pressure can be used, as long as it is a continuous function. In order to find the coefficients, the following integral is to be evaluated

$$\mathrm{S}_{PP}(\alpha_m,\alpha_n)=\frac{1}{2L_x}\frac{1}{2L_y}\int_{-L_x}^{L_x}\int_{-L_y}^{L_y}\frac{S_{pp}(\xi_x,\xi_y)}{\Phi_{pp}(\omega)}\,\mathrm{e}^{-\mathrm{i}\alpha_m\xi_x}\mathrm{e}^{-\mathrm{i}\alpha_n\xi_y}\,\mathrm{d}\xi_y\,\mathrm{d}\xi_x, \tag{37}$$

where $S_{pp}(\xi_x,\xi_y)$ is defined by either Eq. (25) or Eq. (26). Dividing the area into M' and N' segments and using a trapezoidal approximation to the integral, yields

$$\begin{aligned}\mathrm{S}_{PP}(\alpha_m,\alpha_n)\approx{}&\frac{\Delta_x}{2L_x}\frac{\Delta_y}{2L_y}\,\mathrm{e}^{\mathrm{i}\alpha_m L_x}\mathrm{e}^{\mathrm{i}\alpha_n L_y}\\&\times\sum_{m'=0}^{M'}\sum_{n'=0}^{N'}a'_m a'_n S_{pp}(-L_x+m'\Delta_x,-L_y+n'\Delta_y)\mathrm{e}^{-\mathrm{i}\alpha_m m'\Delta_x}\mathrm{e}^{-\mathrm{i}\alpha_n n'\Delta_y},\end{aligned} \tag{38}$$

where $\Delta_x=2L_x/(M')$ and $\Delta_y=2L_y/(N')$. a'_m is unity if not $m'=0$ or $m'=M'$, in which case it is $\frac{1}{2}$. A similar relation holds for a'_n. The double sum is on a form that can be evaluated efficiently using an FFT, implemented in for example MATLAB. Due to possible aliasing distortion, it is important to choose M' and N' large enough at a given frequency.

3.3. Cross-spectral density of the response

The series in Eq. (35) is inserted into integral (22) and the order of summation and integration interchanged

$$\begin{aligned}S_{ww}(\mathbf{r}_1,\mathbf{r}_2,\omega)&=\Phi_{pp}(\omega)\sum_m\sum_n\mathrm{S}_{PP}(\alpha_m,\alpha_n)\\&\quad\times\int_S\int_S(H(\mathbf{r}_1,\mathbf{s}_1,\omega)\mathrm{e}^{-\mathrm{i}\alpha_m x_{s1}}\mathrm{e}^{-\mathrm{i}\alpha_n y_{s1}})^*(H(\mathbf{r}_2,\mathbf{s}_2,\omega)\mathrm{e}^{-\mathrm{i}\alpha_m x_{s2}}\mathrm{e}^{-\mathrm{i}\alpha_n y_{s2}})\,\mathrm{d}\mathbf{s}_1\,\mathrm{d}\mathbf{s}_2\\&=\Phi_{pp}(\omega)\sum_m\sum_n\mathrm{S}_{PP}(\alpha_m,\alpha_n)G^*(\mathbf{r}_1,\alpha_m,\alpha_n,\omega)G(\mathbf{r}_2,\alpha_m,\alpha_n,\omega).\end{aligned} \tag{39}$$

The definitions of the sensitivity function in Eq. (21) was used. This function describes the response to a travelling pressure wave and was previously calculated with the SSEM in Section 2. Considering only the auto-spectral density of the response at location $\mathbf{r}$ gives specifically

$$S_{ww}(\mathbf{r},\mathbf{r},\omega)=\Phi_{pp}(\omega)\sum_m\sum_n\mathrm{S}_{PP}(\alpha_m,\alpha_n)|G(\mathbf{r},\alpha_m,\alpha_n,\omega)|^2. \tag{40}$$

4. Validation and comparison with measurements

In this section, predictions, obtained with the presented model, are compared to the results from a detailed conventional FE model and also to experimental results from wind tunnel measurements at the MWL in Stockholm.

The anechoic wind tunnel was designed to minimize acoustic contamination as described in Ref. [9] and assessed in Ref. [12]. The plate acceleration was measured at five different locations

by light weight accelerometers attached to the plate, whereas the cross-spectral density of the wall pressure was measured with two spatially separated 1/8-inch microphones, see Ref. [9].

4.1. Measurement setup

A number of wind tunnel measurements were made for flow speeds ranging from 80 up to 120 m/s, but for brevity only the results for 100 m/s will be discussed here. Similar trends were also observed for the other flow speeds. Three different plate structures could be flush-mounted in a test section located in a reverberation chamber. One of them was described in Ref. [1] as test case (b) and another was a clamped plate with damping patches attached to it.

The plate studied here was a clamped aluminum plate with a length L_x of 76.8 cm, a width L_y of 32.8 cm, a thickness h of 1.6 mm, a Young's modulus E of 7e10 $\mathrm{N/m^2}$, a density ρ of 2700 $\mathrm{kg/m^3}$ and a Poisson ratio equal to 0.33. With the wind tunnel in use at different flow speeds, a shaker was used to make the plate vibrate at levels far exceeding those caused by the turbulence. The shaker was then turned off and from measuring the decay in vibration, the plate loss factors in octave bands could be determined and are given in Table 2. This damping was included in the element formulation with a complex Young's modulus $E(1+\mathrm{i}\eta)$, where η for a given frequency was found as a linear interpolation between the measured octave band values for the loss factors.

4.2. Vibration response

A non-dimensional metric R for the response of the plate was defined in order to compare the vibration response to turbulence excitation

$$R = \frac{\omega^2 \rho^2 h^2 S_{vv}}{\Phi_{pp}}, \tag{41}$$

where ρ and h are density and thickness of the plate, respectively. S_{vv} is the cross-spectral density of the velocity. The response calculated and discussed here is an average of the response at five positions of the plate, see Table 3. For the SSEM, 18 strip elements were used in the derivation of one super element.

The presented method was validated against results provided by Ulf Tengzelius (FOI) using a finite element method with 56×24 elements and Eq. (22). Fig. 2 shows the result for the metric R. For this special figure a Young's modulus of 6.6e10 $\mathrm{N/m^2}$ and a Poisson ratio of 0.31 was used. The frequency resolution was only 3 Hz, which is too wide to completely resolve the resonances at low frequencies. Both methods used the modified Corcos model and the results show good agreement.

Table 2
Measured loss factor for a flow speed of 100 m/s

Octave band (Hz)	125	250	500	1000	2000
Loss factor	0.045	0.006	0.006	0.005	0.003

Table 3
Positions of measured and predicted plate response

x (m)	0.134	0.224	0.334	0.499	0.634
y (m)	0.284	0.089	0.184	0.229	0.119

Note: Plate is located in the xy plane with the origin placed in one corner.

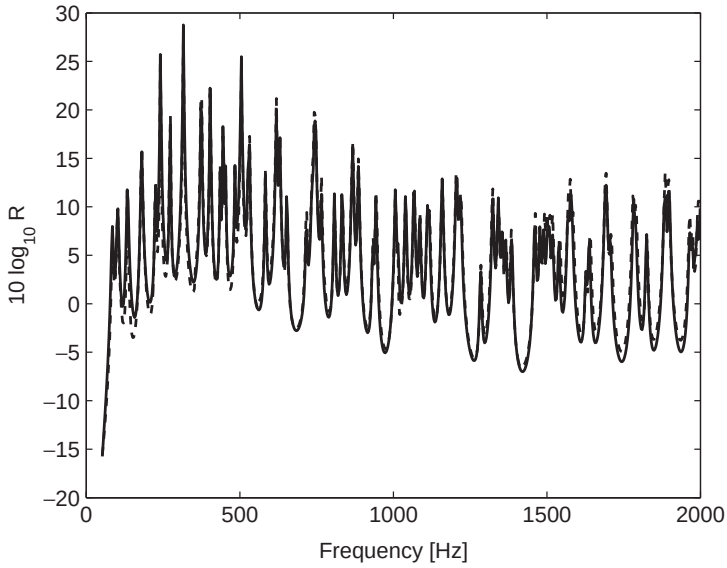

Fig. 2. Non-dimensional vibration response for a clamped plate excited by turbulent flow with a free flow velocity of 100 m/s. Solid line, FEM calculations; dashed line, presented method.

Figs. 3 and 4 compare the calculated and measured metric R for a free flow velocity of 100 m/s in narrow-bands of width 6.25 Hz. The frequency resolution with the SSEM was less than 0.5 Hz at low frequencies. This ensured that the resonance peaks were resolved, before integrating to the 6.25 Hz bandwidth. As can be seen there is a similar good agreement between measurements and predictions with both the Corcos- and Chase-like models up to around 800 Hz. The reason for this being that they model the wavenumber domain close to the convective peak [9] in a similar fashion. Thus, as long as the frequency is around the aerodynamic coincidence frequency, which for the investigated case was at 370 Hz, the predicted response will not differ much. However, above this frequency, the low wavenumber description of the wall pressure becomes increasingly important for the response. For example as discussed in Refs. [9,13], Chase's model seems to model this domain better. Fig. 5 compares the results of Figs. 3 and 4 in third octave bands and an average difference of 3 dB was found using the modified Chase model. To the authors' knowledge this accuracy of the predicted plate response to TBL excitation is one of the best to be found in the literature so far.

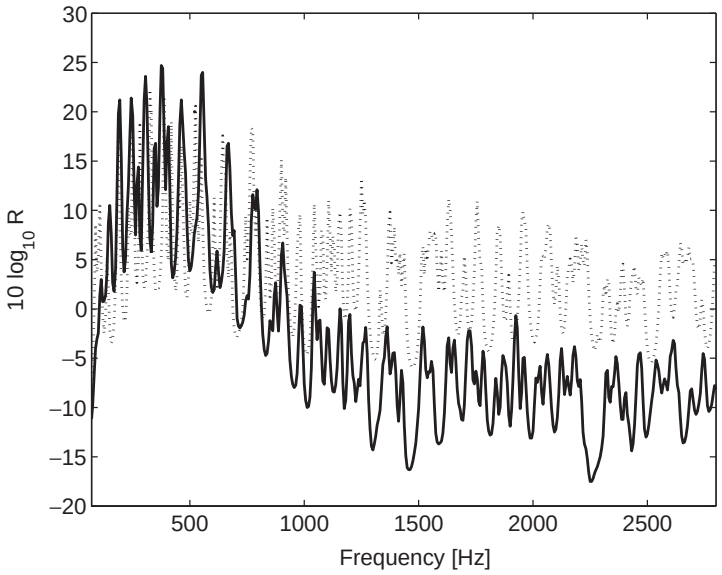

Fig. 3. Non-dimensional vibration response for a clamped plate excited by turbulent flow with a free flow velocity of 100 m/s. Solid line, measurements; dotted line, predictions with the SSEM using a modified Corcos model.

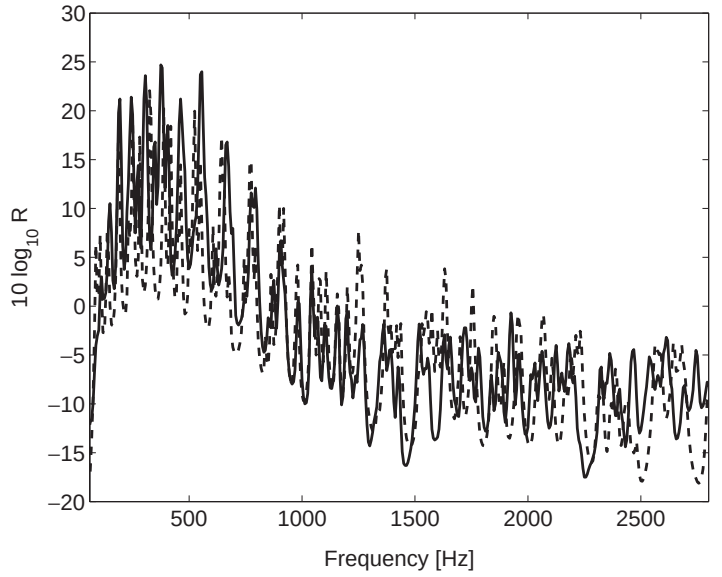

Fig. 4. Non-dimensional vibration response for a clamped plate excited by turbulent flow with a free flow velocity of 100 m/s. Solid line, measurements; dashed line, predictions with the SSEM using a modified Chase model.

A 3 mm static deflection of the plate, caused by a static pressure difference between the inside and outside of the tunnel, was observed for a free flow velocity of 100 m/s. This introduced a pre-stress $N_{x,y}$ in the x- and y-direction of the plate, which was modelled using $N_{x,y} \approx$

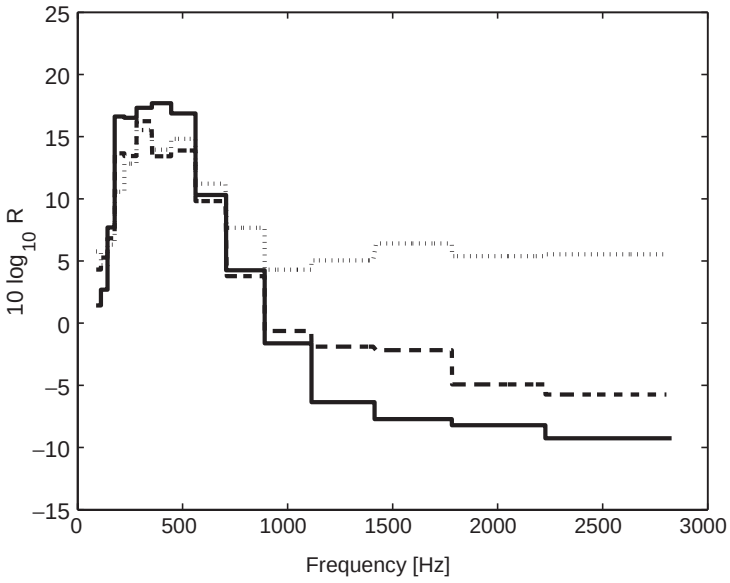

Fig. 5. Non-dimensional vibration response in 1/3-octave bands. Solid, measurements; dashed, results based on modified Chase; dotted, results based on modified Corcos.

$2Eh(0.003\text{m})^2/L_{x,y}^2$. The effect of this pre-stress for the response predictions was mainly to shift the resonance frequencies slightly upwards, especially at lower frequencies. For the third octave band power, however, the effect was only of the order of one dB or less and therefore these results are not commented on further here. Other possible errors in the model exist, e.g. the neglect of curvature and uncertain boundary conditions. The estimated damping loss factor will also contain errors that contribute to the overall error. Although work has been done to extend the study to include other types of boundaries and account for the curvature of the plate, more work undoubtedly remains, if the model is to become even more accurate.

5. Conclusion

In this paper, the spectral super element formulation presented in an accompanying paper was extended to account for distributed forces and then validated against an exact spectral finite element method. The response to a travelling pressure wave was then used in combination with a wavenumber frequency description of the wall pressure field to predict the TBL induced response of a clamped plate. The formulation was validated against a detailed conventional FE model, showing an excellent agreement. Modified Corcos- and Chase-like models were derived in a previous paper [9] in order to model the measured wall pressure data. With both these models quite a good agreement to measured plate response was obtained close to and below the aerodynamic coincidence, whereas the modified Chase model provided a better agreement at high frequencies.

Acknowledgements

This work was supported by the European Commission, ENABLE (GRD4_CT-00-00223) and the Swedish Research Council (621-2002-5661). Many thanks to Urmas Ross for providing measurement results and to Ulf Tengzelius for his FE calculation.

References

[1] F. Birgersson, S. Finnveden, C.-M. Nilsson, A spectral super element for modelling of plate vibration. Part 1: general theory, *Journal of Sound and Vibration* 287 (2005) 297–314, this issue.
[2] D.E. Newland, *An Introduction to Random Vibration and Spectral Analysis*, Longman, New York, 1984.
[3] Y.K. Lin, *Probabilistic Theory of Structural Dynamics*, McGraw-Hill, New York, 1967.
[4] F. Birgersson, N.S. Ferguson, S. Finnveden, Application of the spectral finite element method to turbulent boundary layer induced vibration of plates, *Journal of Sound and Vibration* 259 (2003) 873–891.
[5] C. Maury, P. Gardonio, S.J. Elliott, A wavenumber approach to modelling the response of a randomly excited panel—part i: general theory, *Journal of Sound and Vibration* 252 (2002) 83–113.
[6] F. Birgersson, S. Finnveden, G. Robert, Modelling turbulence induced vibration of pipes with a spectral finite element method, *Journal of Sound and Vibration* 278 (2004) 749–772.
[7] D.M. Chase, Modelling the wavevector-frequency spectrum of turbulent boundary layer wall-pressure, *Journal of Sound and Vibration* 70 (1980) 29–67.
[8] G.M. Corcos, The structure of the turbulent pressure field in boundary layer flows, *Journal of Fluid Mechanics* 18 (3) (1964) 353–378.
[9] S. Finnveden, F. Birgersson, U. Ross, T. Kremer, A model for wall pressure correlation for prediction of turbulence induced vibration, *Journal of Fluids and Structures*, submitted.
[10] R.S. Langley, Application of the dynamic stiffness method to the free and forced vibration of aircraft panels, *Journal of Sound and Vibration* 135 (1989) 319–331.
[11] B.M. Efimtsov, Characteristics of the field of turbulent wall pressure fluctuations at large Reynolds numbers, *Soviet Physics—Acoustics* 28 (4) (1982) 289–292.
[12] S. Finnveden, Formulas for modal density and for input power from mechanical and fluid point sources in fluid filled pipes, *Journal of Sound and Vibration* 208 (1997) 705–728.
[13] A.O. Borisyuk, V.T. Grinchenko, Vibration and noise generation by elastic elements excited by a turbulent flow, *Journal of Sound and Vibration* 204 (1997) 213–237.